Parametric Resonant Control of Macroscopic Behaviors of Multiple Oscillators

Pengcheng Xie[1] and Molei Tao[2]

Abstract— **Consider a finite collection of oscillators, which a user has limited means to perturb due to physical restrictions. We show that as long as the stiffness parameters of these oscillators can be harmonically perturbed, one can design a single shared perturbation, such that macroscopic trajectory tracking is achieved independently in each oscillator; that is, the oscillation amplitudes of all oscillators will approximate, respectively, an arbitrary collection of target functions. This control mechanism is based on the dynamical phenomenon of parametric resonance, which not only permits both increase and decrease of the oscillation amplitude by design, but also the simultaneous control of multiple oscillators with distinct intrinsic frequencies. A simulated animation of a remotely-powered-and-controlled array of circuits illustrates the efficacy of this control. Oscillators that can be controlled by this mechanism are not limited to harmonic ones, but those subject to additional weak damping, noise, and nonlinearity.**

I. Introduction

Our abilities to interact with practical systems are constrained by physical and technological limitations; in particular, this article considers a setup whose goal is to control the oscillation amplitudes (and hence the energies) of a group of oscillators, but each oscillator can only be perturbed in a restricted, parametric way. A theoretical approach will be proposed to individually control the behaviors of all oscillators by a single shared signal, based on a dynamical phenomenon known as parametric resonance [1][2]. The main result is, when the intrinsic frequencies of the oscillators are separated, the energy/amplitude of each oscillator can be made to well-approximate an arbitrary positive slowly varying target function. Throughout this article, this type of objective will be called macroscopic trajectory tracking.

One motivation of this study is a recent progress in the development of wireless energy transferring technologies, termed capacitive parametric ultrasound transductor (CPUT; see [3], [4], [5]). CPUT is based on an *RLC* circuit, where one of the capacitor's double plates is a membrane that can be mechanically modulated by an external ultrasound signal, and the ultrasound is designed to vary the capacitance (and hence the stiffness parameter of the *RLC* oscillator) in a specific way such that the circuit is resonantly excited. In this manner, the mechanical energy of the ultrasound is wirelessly transferred into the electric energy of the circuit, supporting the operation of its load, which could be, for instance, implanted biomedical devices (see e.g. [6] and [7] for pioneer work prior to CPUT, and [3], [4] for the applicability of CPUT). Therefore, CPUT provides an example in which the oscillator can and only can be nonintrusively perturbed in its stiffness parameter. There are other practical setups that have similar constraint and objective. For instance, the coupling between an external laser-induced oscillatory electromagnetic field and the nonlinear core of an inductor (e.g., [8]) can provide another source of parametric excitation of electric circuits. See Fig. 1 for a cartoon of these two setups. One advantage of these setups is that the perturbation is essentially remote and wireless. Meanwhile, it should be mentioned that the setup does not have to be electrical or electromechanical, and there are mechanical analogies: for instance, the energy contained in mechanical vibrations has also been successfully harvested in experiments based on spring-mass systems (e.g., [9]), and mechanical vibrations that vary the effective lengths of springs will correspond to a purely mechanical way of producing parametric excitations of oscillators, just like how a child pumps a swing. Additional magnetic analogies will also be reviewed near the end of this section.

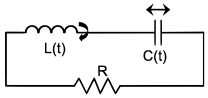

Fig. 1: *RLC* circuit with variable capacitance due to variations in double plate distance, and/or variable inductance due to fastening/loosening of the coil. No power source is needed.

These setups are relevant because the mechanism proposed in this article can lead to the remote control of the corresponding oscillators. In all aforementioned work, resonance was used to inject energy into such a system. We suggest using the same form of restricted parametric perturbations to accomplish (i) a more refined objective, which is macroscopic trajectory tracking, and (ii) the simultaneous control of many such systems by a shared signal, for instance via an incident acoustic wave or electromagnetic field. This will allow, for instance, the wireless manipulation of an array of *RLC* circuits with one common external signal, without interrupting the operation of the circuits. Potential applications are not limited to biomedical ones, but also possibly a centralized operation of a swarm of microscopic robots, for example. However, we clarify that the scope of this short article is restricted to a mathematical demonstration, in a simplified setup, of the resonant control mechanism only.

Specifically, consider a system of oscillators subject to

*Molei Tao thanks Shuo Han for insightful comments and the support of NSF grants DMS-1521667, ECCS-1829821, and DMS-1847802

[1]Pengcheng Xie is with Xian Jiaotong Univ., and this work was primarily done while he was an exchange student at Georgia Institute of Technology

[2]Molei Tao is with School of Mathematics, Georgia Institute of Technology, USA mtao@gatech.edu

weak dissipation, weak nonlinearity (chosen to be cubic just for illustration purposes), and small white noise:

$$\begin{cases} dq_i = v_i dt & i = 1, \cdots, n \\ dv_i = -\left(\omega_i^2(1+P(t))q_i(t) + \mu_i q_i^3 + \gamma_i v_i\right) dt + \sigma_i dW_i \end{cases} \tag{1}$$

where q_i, v_i, ω_i, μ_i, γ_i and σ_i are respectively ith oscillator's position, velocity, intrinsic frequency, strength of small nonlinearity, damping coefficient, and small noise amplitude. The oscillators' stiffness (i.e. ω_i^2) are perturbed in time by $P(t)$, which is chosen as

$$P(t) = \sum_{i=1}^{n} \varepsilon_i \cos(2\omega_i t + \theta_i). \tag{2}$$

Assume ω_i's are all distinct, because in many applications one designs the oscillators in order to accomplish a certain task, and in this case s/he can choose ω_i values to be isolated.

Given an arbitrary family of positive-valued functions of time $\{f_i(t)\}_{i=1}^n$ that are slowly varying[1], we will choose θ_i and small ε_i as piecewise constant functions of time, such that the amplitude of each oscillator, defined by $\sqrt{q_i(t)^2 + \dot{q}_i(t)^2/\omega_i^2}$, approximates the corresponding target function $f_i(t)$ when the damping, nonlinearity and noise are weak. More precisely, let ε be such that $\varepsilon_i(t) \leq \varepsilon$ for all i and t, and $\omega = \min_i \omega_i$. Then when noise is absent, the pointwise (i.e. strong) accuracy of this approximation is

$$\sqrt{q_i(t)^2 + \dot{q}_i(t)^2/\omega_i^2} - f_i(t) = \mathscr{O}(\varepsilon) \tag{3}$$

for all bounded t except in a transient initialization phase (corresponding to $t \ll \varepsilon/\omega$); the same result holds with high probability when there is noise.

Details of how to choose ε_i and θ_i will be given by Algorithm 1. The physical meaning of these choices is, one chooses the parametric perturbation as a linear combination of small-amplitude harmonics, and carefully alters the frequencies and amplitudes of these harmonics only once in a while. Such choices are implementable at least when the control signal is a generated ultrasound or laser. Numerical simulations, including an animation, will be provided to illustrate the efficacy of this algorithm.

Derivations that lead to Algorithm 1 will be described. The design rationale is based on the idea of resonant control, which utilizes the selectivity of resonance in frequencies. Since one can design the circuits such that all their intrinsic frequencies are distinct, components with different frequencies in the perturbation $P(t)$ can be used to control different circuits in parallel. Important to note is, superimposing multiple frequencies for achieving multiple objectives is not new but a classical idea; nevertheless, the particular choice of using parametric resonance to accomplish each objective is innovative. Unlike linear resonance, parametric resonance can be used to induce not only an increase in the energy/amplitude but also a decrease. Only by enabling both growth and decay can trajectory tracking be accomplished.

Trajectory tracking is achieved only at a macroscopic timescale. Due to its restricted form, the control $P(t)$ is unable to alter the short time behavior of the system, which will always be nearly harmonic oscillations; nevertheless, the accumulated interaction between the parametric perturbation and the intrinsic oscillations will eventually lead to an effective contribution across timescales, which we utilize to enable the tracking of arbitrary function at a timescale slower than the oscillation timescale. Being able to trajectory-track only at the macroscopic timescale is, in many cases, not a critical limitation, because as long as all $\omega_i \gg 1$ this macroscopic timescale is actually $\mathscr{O}(1)$, and often one can design the circuits to have high intrinsic frequencies. Also needed mentioning is, macroscopic trajectory tracking is not a new idea but the objective of the classical problem of amplitude modulation. What is new is again the mechanism that accomplishes it (parametric resonance). Also, because many amplitudes are simultaneously modulated, a trajectory in a high-dimensional space is being tracked, and hence the name.

As the proposed approach utilizes small scales to control large scale behaviors, it is an application of the recently proposed multiscale control methodology (see e.g., [11], [10]). It complements the traditional Lie-algebra-based nonlinear controllability theory (e.g., [12]), which alone is insufficient because (i) the goal of trajectory-tracking is stronger than the notion of controllability, and (ii) the controlled system has microscopic details, and while these details (and thus the entire system) are not controllable, it is still possible to control only the macroscopic behavior. A technical sidenote is, it is only a matter of definition whether to call the $\mu_i = 0, \sigma_i = 0$ system linear, because it can be viewed as both a nonautonomous linear system and a nonlinear system if time is viewed as a dummy variable satisfying $\dot{t} = 1$.

Motivated by rich applications, there have been long time and deep investigations in the problem of controlling many similar oscillators by one shared signal. For instance, the active field of ensemble control is concerned with the controllability of infinitely many structurally-alike oscillators, which originated from practical problems such as how to manipulate an ensemble of nuclear spins. To be more specific, Bloch equation [13], for instance, which is essential to applications such as nuclear magnetic resonance (NMR) spectroscopy and magnetic resonance imaging (MRI), has its governing differential equations being linear with designable time-dependent coefficients similar to our setup, and [14] discussed its ensemble control. We also refer to [15] and [16], respectively, for more theoretical and numerical investigations in ensemble control. Our study is complementary to ensemble control in the sense that we only control finitely many oscillators, but because of that simplification, each oscillator can be controlled more closely (recall the difference between macroscopic trajectory-tracking and controllability). There are many other applications of controlling multiple oscillators in which a quasiperiodic control enters the system in an affine way. For example, see [17] for how such control

[1]Defined as f_i changing at a timescale slower than the oscillation timescale associated with ω_i; see [10] for more details. When $\omega_i \gg 1$ the function only has to be sufficiently smooth to be slowly varying.

was designed to steer, both theoretically and experimentally, electrochemical reactions into synchronization; this objective was not the same as trajectory-tracking, but the work was remarkable because the system is nonlinear and real-world. We also refer to [18], [19], [20], [21], [22], [23], [24], [25], [25], [26] and references therein for additional interesting discussions on the control aspect of oscillator synchronization. We repeat, however, that the main purpose of this article is simultaneous trajectory-tracking, not synchronization.

II. Control of multiple oscillators: the time-dependent linear theory

Consider a system of n oscillators

$$\ddot{q}_i(t)+\omega_i^2(1+P(t))q_i(t)+\gamma_i\dot{q}_i(t)=0,\quad i=1,2,\cdots,n \quad (4)$$

where γ_i's are constant parameters that characterize the strengths of damping, which model ubiquitous dissipation in practical systems, and

$$P(t)=\sum_{i=1}^{n}\varepsilon_i\cos(\omega_i' t+\theta_i)$$

is a shared, implementable (see Introduction) quasiperiodic perturbation to the stiffness parameters of all oscillators, which will be the control to be designed. Parametrically perturbed *RLC* circuits are natural examples of such systems.

We will show, via Theorem 1, that the choice of $\omega_i'=2\omega_i$ for all i will achieve parametric resonance in each oscillator, and this choice will be assumed from now on. Theorem 1 will also quantify how ε_i and θ_i values affect the macroscopic behaviors of the oscillators, which will later on allow us to design $P(t)$ for achieving macroscopic trajectory tracking in each of these oscillators.

The following weak dissipation assumption will be made. It is a reasonable assumption because after all only underdamped oscillators are truly oscillatory.

Condition 1. Assume $0\le\gamma_i\ll\omega_i$.

A. The Asymptotic Analysis

Theorem 1. Consider (4) with $P(t)=\sum_{i=1}^{n}\varepsilon_i\cos(2\omega_i t+\theta_i)$, where all ω_i's are distinct and Condition 1 is satisfied. Given $\varepsilon_i\ll 1$, there exists C such that for $0\le t\le\frac{C}{\varepsilon_i}$:

when $$\tan\frac{\theta_i}{2}=\frac{2\hat{\omega}_i q_i(0)+\gamma_i q_i(0)+2\dot{q}_i(0)}{-2\hat{\omega}_i q_i(0)+\gamma_i q_i(0)+2\dot{q}_i(0)},$$

the ith oscillator's solution is

$$q_i(t)=e^{\frac{\varepsilon_i\hat{\omega}_i t}{4}-\frac{\gamma_i}{2}t}\left(q_i(0)\cos(\hat{\omega}_i t)+\dot{q}_i(0)\frac{\sin(\hat{\omega}_i t)}{\omega_i}\right)+\mathscr{O}(\varepsilon_i).$$

and when $$\tan\frac{\theta_i}{2}=\frac{2\hat{\omega}_i q_i(0)-\gamma_i q_i(0)-2\dot{q}_i(0)}{2\hat{\omega}_i q_i(0)+\gamma_i q_i(0)+2\dot{q}_i(0)},$$

the solution is

$$q_i(t)=e^{-\frac{\varepsilon_i\hat{\omega}_i}{4}t-\frac{\gamma_i}{2}t}\left(q_i(0)\cos(\hat{\omega}_i t)+\dot{q}_i(0)\frac{\sin(\hat{\omega}_i t)}{\omega_i}\right)+\mathscr{O}(\varepsilon_i),$$

Here $\hat{\omega}_i=\sqrt{\omega_i^2-\gamma_i^2/4}$.

The implications of Theorem 1 are, (i) what affects the ith oscillator in $P(t)$ is only the term with two-times the oscillator frequency, and (ii) a particular choice of phase value in that term will lead to an exponential decay of the amplitude of that oscillator, and another choice will lead to an exponential growth of the amplitude. Once one can let the amplitude grow and decay at times of choice, macroscopic trajectory tracking becomes a possibility. In addition, because of (i), one only needs to design the a term in $P(t)$ that controls oscillator #i, and then linearly combine all terms to parallelly control all the oscillators.

The proof is in the APPENDIX.

B. The Algorithm for Designing the Control $P(t)$

How to choose piecewise-constant perturbation amplitude and phase for the macroscopic trajectory-tracking of a single, frictionless harmonic oscillator has been described by Algorithm 16 in [10]. Theorem 1 showed it suffices to control each oscillator separately by designing the corresponding ε_i and θ_i. Therefore, we only need to generalize the existing algorithm to the dissipative case based on the special choices of θ_i given by Theorem 1.

The idea is, to track $f_i(t)$, approximate it by a piecewise exponential function, and choose fixed ε_i and θ_i values within each time piece, so that the amplitude of the ith oscillator mimics the exponential behavior of f_i on that piece.

This piecewise approach will be accurate as long as f_i changes much slower than oscillations at the intrinsic frequency ω_i, which is a mild requirement because ω_i can be large. More precisely:

Condition 2. Assume that each $f_i(t)\in\{f_i(t)\}_{i=1}^{n}$ is slowly varying when compared to the time scale $0<\max\{1/\omega_i\}<\infty$, which means that $f_i(t)\in C^1([0,T])$ and

$$|\frac{1}{\omega_i}\frac{d}{dt}log f_i(t)|\ll 1\quad and\quad |\frac{1}{\omega_i}\frac{d}{dt}f_i(t)|\ll 1$$

for all $t\in[0,T]$, where T is the end time of the control.

Under Condition 1 & 2, the following will provide $P(t)$ so that each oscillator tracks its corresponding f_i:

Algorithm 1 Parametric resonant control of oscillators

1: Discretize the time axis into uniform pieces, with width (i.e., time step, which is chosen to be between fast oscillation timescales and the macroscopic tracking timescale) $H:=\frac{C}{\min\{\omega_i\}}$ for some pre-chosen $\mathscr{O}(1)$ constant C (default: $C=2$).

2: At the beginning of each time step (i.e., $t=mH$ for $m\in\mathbb{N}$), compute for each oscillator ($i=1,\cdots,n$),

$$r_i:=\frac{f_i(t+H)}{\sqrt{q_i(t)^2+\dot{q}_i(t)^2/\omega_i^2}} \quad (5)$$

3: Case 1: If $r_i \geq 1$ (exponential growth needed), let

$$\varepsilon_i = \frac{4\log r_i + 2\gamma_i}{\omega_i H}$$
$$\theta_i = 2\arctan\frac{2\hat{\omega}_i q_i(0) + \gamma_i q_i(0) + 2\dot{q}_i(0)}{-2\hat{\omega}_i q_i(0) + \gamma_i q_i(0) + 2\dot{q}_i(0)}$$

throughout this time step (i.e., for $t \in [mH, (m+1)H)$).

4: Case 2: If $r_i \leq 1$ (exponential decay needed), let

$$\varepsilon_i = -\frac{4\log r_i + 2\gamma_i}{\omega_i H}$$
$$\theta_i = 2\arctan\frac{2\hat{\omega}_i q_i(0) - \gamma_i q_i(0) - 2\dot{q}_i(0)}{2\hat{\omega}_i q_i(0) + \gamma_i q_i(0) + 2\dot{q}_i(0)}$$

throughout this time step.

5: Let $P(t) = \sum_i \varepsilon_i \cos(2\omega_i t + \theta_i)$ throughout this time step.

6: Move to the next time piece (i.e., $m \to m+1$) and iterate until $m = \lfloor T/H \rfloor$.

Remark. *(arbitrary initial condition)* The initial energy of the system has to be nonzero for the parametric resonant control to work, but it can be arbitrarily small. If there is noise, even zero initial energy is no longer an issue, because the noise will perturb the energy away from zero and such perturbation 'ignites' the parametric resonance.

Remark. *(slow variation leads to accuracy)* Conditions 1 & 2 together ensure $\varepsilon_i \ll 1$. They are critical because we would like to choose ε_i such that when a growth in the oscillation amplitude is needed, enough energy can be injected into the circuit even though there is dissipation, but ε_i cannot be too large, not only because the asymptotic analysis is based on the assumption of small ε_i, but also because physically there is a limitation on the rate of energy injection. More precisely, we require $\varepsilon_i \ll 1$ to satisfy $\frac{\varepsilon_i \hat{\omega}_i t}{4} - \frac{\gamma_i t}{2} = \log r_i$ when $r_i > 1$, and Condition 1 & 2 together fulfill this requirement.

Importantly, if one would like to reduce ε to improve the accuracy of macroscopic trajectory tracking (see (3); recall $\varepsilon \geq \varepsilon_i(t)$), increasing all ω_i's while f_i's are fixed will provide such a reduction.

Remark. *(closed-, open-loop, and stability)* It is easy to see, for instance from (5), that Algorithm 1 corresponds to a closed-loop control. It assumes that precise measurements of the state of the system at discrete time points mH are possible. This is a limitation of our approach. Fortunately, some degrees of relaxation are allowed: if one only knows the initial state of the system, an open-loop control based on

$$r_i := f_i(t+H)/f_i(t)$$

can be used to replace (5), and $q_i, \dot{q}_i$ will just be simulated. However, this choice will lead to accumulations of errors when ω_i's are not large.

If inexact state estimation is available, more errors will be induced; however, if q_i,$\dot{q}_i$ can be estimated with $\mathscr{O}(\varepsilon)$ error, the error of trajectory tracking will still be bounded by $\mathscr{O}(\varepsilon)$ as in (3) for the case of exact measurements. On the other hand, the algorithm is not expected to work if only the initial state is known but with error exceeding $\mathscr{O}(\varepsilon)$.

C. Animated Illustration of The Simultaneous Macroscopic Trajectory Tracking

To demonstrate the efficacy of our methodology, we consider controlling the luminosities of an array of light bulbs. Each light bulb (assumed of constant resistance) is the load of an *RLC* circuit and tunable in terms of brightness. By simultaneously trajectory-tracking the energy in each circuit, one can turn the array into a miniaturized monitor, which can display contents according to a remote control without requiring a power cord or a signal cord. This is illustrated by a produced animation.

More precisely, we pre-chose the target functions $f_i(t)$ and numerically simulated (4) with $P(t)$ given by Algorithm 1. Time variations of the array were outputted as an animation (available at `https://youtu.be/JmSLcOl_7MY` ; see also Fig. 2). In this animation, each frame consists of $5 \times 12 = 60$ blocks, and the grey scale of each block corresponds to a bulb luminosity given by the oscillation amplitude in that block, which varies in time. By making the amplitudes of 60 oscillators follow different target functions (see APPENDIX for details), we command *GT*, which is an abbreviated name of the authors' institute, to enter from the right side, then disappear one by one and appear again in the order of handwriting. Fig. 3) illustrates the nontrivial $P(t)$ used to track such a trajectory.

Fig. 2: Snapshots of an animation that illustrates the simultaneous control of oscillators: each oscillator is a pixel. Time instances of these 4 snapshots: 0:02, 0:06, 0:07, 0:10.

This animation provides an illustration of the following features of the proposed control mechanism:

- With a single shared control function $P(t)$, a large amount of oscillators can be individually controlled.
- This control also powers all the oscillators at the same time.
- In addition to increasing, the amplitudes of the oscillators can also decrease by design. This is necessary for enabling trajectory tracking. Moreover, different

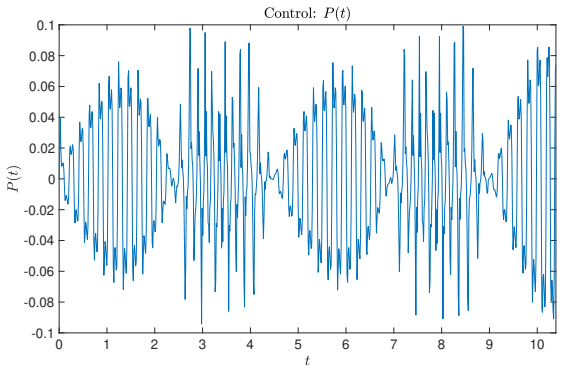

Fig. 3: The control $P(t)$ used for producing the animation.

oscillators can behave independently; e.g., some can decrease while others are increasing (all by design).

- When all of the intrinsic frequencies are large, the system responses fast and the control is accurate too.

D. Static Illustration of Simultaneous Macroscopic Tracking

We demonstrate Algorithm 1 on a system of four damped oscillators. The target functions are arbitrarily chosen as

$$\begin{cases} f_1(t) = 0.1t^2 + (13-t) + t\sin t + e^{-t} \\ f_2(t) = 2t\cos(2t) + t + 10 \\ f_3(t) = \dfrac{1}{2}t + \dfrac{1}{2}t\sin t + 13 + 10e^{-2t} \\ f_4(t) = 0.1t^2 + t\cos t + 10 + 2e^{-t} - t \end{cases} . \tag{6}$$

The initial condition is arbitrarily chosen to be $q_i(0) = 10, \dot{q}_i(0) = 0$ for $i = 1,2,3,4$. Choices of parameters of the oscillators are listed in TABLE I.

TABLE I: Parameters of damped oscillators in Section II-D

ω_1	ω_2	ω_3	ω_4	γ_1	γ_2	γ_3	γ_4
280	290	300	310	4.5	5	5.5	6

Numerically integrated trajectories of $q_i(t)$ are shown in Fig. 4, which confirms the accomplishment of macroscopic trajectory tracking.

As a comparison, Fig. 5 shows that if we choose ε_i and θ_i using the frictionless algorithm in [10], which corresponds to the frictionless case of Theorem 1's conclusion, then the control does not work any more, even though γ_i's are small. Thus algorithm 1 which incorporates the leading order effect of γ_i is indispensable in a workable generalization.

III. The Case with Additional Nonlinearity and White Noise

Since practical systems are seldom linear deterministic, we now demonstrate that the same multiscale resonant control algorithm also applies to systems with weak noise and nonlinearity, as long as the target functions have reasonable magnitudes, and 'reasonable' will be quantified.

Consider the multiple oscillator system with additional nonlinear forcing terms $\mu_1 q_1^3(t), \mu_2 q_2^3(t), \cdots, \mu_n q_n^3(t)$ and additional Gaussian noises with strength $\sigma_1, \sigma_2, \cdots, \sigma_n$. This

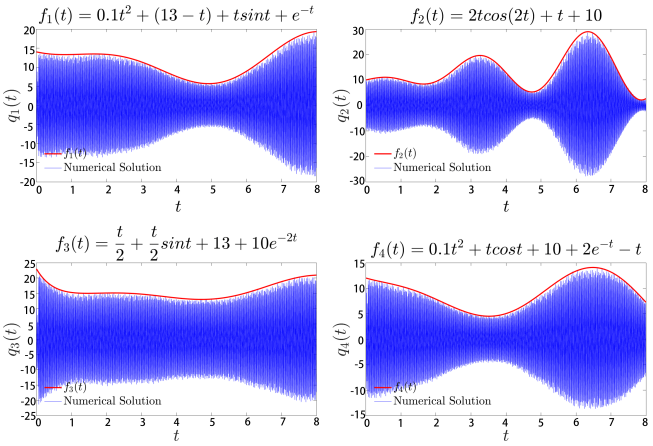

Fig. 4: How oscillations (blue) track the target amplitude functions (red) when four damped oscillators are controlled by Algorithm 1.

cubic nonlinearity is common for mechanical oscillators, e.g., [9]; changing the form of the nonlinearity will affect details of the calculation below, but not the fact that Algorithm 1 still works for reasonable target functions. The governing equations are (1) and the perturbation is of the form (2).

Similar to before, we will focus on one generic oscillator in the system, with intrinsic frequency ω_i. Asymptotic analysis will be employed to estimate how large μ (nonlinearity) and σ (noise) can be such that Algorithm 1 still applies. A proof similar to that of Theorem 1 will also show that if, in addition, all ω_i values are well separated, then a linear combination of perturbations that respectively control each oscillator will simultaneously control all of them. For the sake of length, the detailed calculation will be limited to the frictionless case ($\gamma_i = 0$), but an inspection of the derivation will convince that adding γ will not change the steps or the qualitative conclusion.

A. Asymptotic Analysis for Estimating the Validity Regime

We will quantify how small μ_i and σ_i need to be in order for the nonlinearity and noise to be only a higher

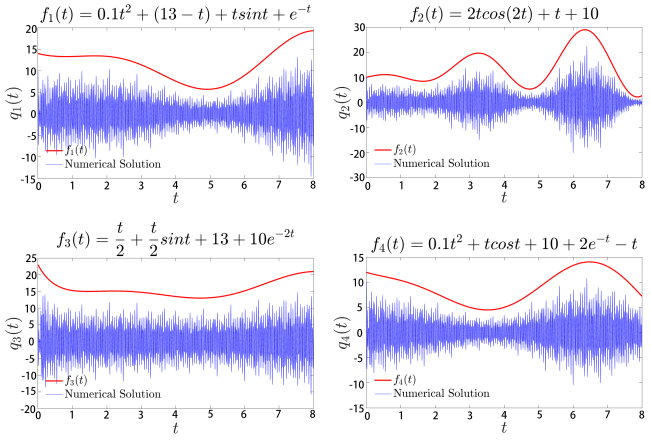

Fig. 5: How oscillations (blue) fail to track the target amplitude functions (red) when four damped oscillators are controlled without correctly considering the damping.

order perturbation to the controlled system. The main tool will be an asymptotic analysis method known as averaging for stochastic differential equations (see e.g., [27]). For conciseness and clarifty, the subscript i will be suppressed in this section unless needed.

For this quantification, write the governing system of equations (1) in the following form

$$dx = (\Omega x + g(x,t))dt + \sigma dW,$$
$$\text{where} \quad \Omega = \begin{bmatrix} 0 & 1 \\ -\omega^2 & -\gamma \end{bmatrix}, \qquad \sigma = \begin{bmatrix} 0 & 0 \\ 0 & \sigma_i \end{bmatrix},$$
$$x = \begin{bmatrix} q \\ p \end{bmatrix}, \qquad g(x,t) = \begin{bmatrix} 0 \\ -\varepsilon\cos(2\omega t)q - \mu q^3 \end{bmatrix}.$$

Large ω and small ε create a separation of scales, but both the fast and the slow scales are mixed in x. We thus introduce a coordinate transformation

$$x(t) = e^{\Omega t} y(t)$$

to separate the scales. In the $\gamma = 0$ case, it spells out as

$$\begin{cases} q(t) = \cos(\omega t)y_1(t) + \frac{\sin(\omega t)}{\omega} y_2(t) \\ p(t) = -\omega\sin(\omega t)y_1(t) + \cos(\omega t)y_2(t) \end{cases}.$$

Ito formula (see e.g.[28]) gives

$$dy = e^{-\Omega t} g(e^{\Omega t} y, t)dt + e^{-\Omega t}\sigma dW, \tag{7}$$

and we will use the method of averaging to obtain a good approximation to the nonlinear equation (7), which is

$$dy = \langle e^{-\Omega t} g(e^{\Omega t} y, t)\rangle dt + \sqrt{\langle e^{-\Omega t}\sigma\sigma^T (e^{-\Omega t})^T\rangle} dB,$$

where $\langle\cdot\rangle$ is a time average defined as

$$\langle h(t)\rangle = \frac{1}{T}\int_0^T h(t)dt$$

and $T = \frac{2\pi}{\omega}$ in our case.

Calculations will show that, for our specific problem, the averaged approximate equation is

$$\begin{cases} dy_1 = -\frac{y_2}{4\omega^2}[\varepsilon - \frac{3(y_1^2\omega^2 + y_2^2)}{2\omega^2}\mu]dt + \frac{\sigma}{\sqrt{2}}\frac{1}{\omega}dB_1 \\ dy_2 = -\frac{y_1}{4}[\varepsilon + \frac{3(y_1^2\omega^2 + y_2^2)}{2\omega^2}\mu]dt + \frac{\sigma}{\sqrt{2}}dB_2 \end{cases}$$

where B_1 and B_2 are i.i.d. standard Wiener processes. Therefore, as long as

$$|\varepsilon| \gg \frac{3(y_1^2\omega^2 + y_2^2)}{2\omega^2}|\mu|, \tag{8}$$

the nonlinearity in the original equation will have negligible impact on the dynamics if the solution is considered only for $\mathcal{O}(\varepsilon^{-1})$ time, and this is indeed the timescale Algorithm 1 is based on.

Note $y_1^2 + \frac{y_2^2}{\omega^2} = q^2 + \frac{p^2}{\omega^2} = A^2$ where A is the oscillation amplitude. Therefore, (8) is equivalent to $|\varepsilon| \gg \frac{3A^2}{2}|\mu|$; that is, $|A| \ll \sqrt{\frac{2|\varepsilon|}{3|\mu|}}$. This means, if the target signal satisfies

$$\max_{t\in[0,T]} |f(t)| \ll \sqrt{\frac{2|\varepsilon|}{3|\mu|}} \tag{9}$$

then tracking $|f|$ can be accomplished from time 0 to T when the nonlinearity is present.

Additionally, in order for the noise not to introduce significant impact on the dynamics (more precisely, in order for the probability of having trajectories significantly different from the deterministic trajectory to be exponentially small [29]), we need the variance of the noise to be much smaller than the norm of the deterministic drift. Note it is the variance, not the amplitude, which can be seen from an asymptotic expansion of the Fokker-Planck equation (e.g., [30]). This leads to an additional condition on the noise strength:

$$\frac{\sigma^2}{2} \ll \min_{t\in[0,T]} |f(t)|\frac{\varepsilon}{4} \tag{10}$$

To summarize, when ω_i is fixed, as μ_i decreases, Algorithm 1 will allow the ith oscillator to track larger functions; on the other hand, as σ_i decreases, it can track smaller (positive) functions. The quantitative relations are given by (9) and (10), and when they hold Algorithm 1 works as if there is no nonlinearity or noise, and with probability exponentially close to one.

Remark. *(robustness)* Similar justification also applies to small unmodeled nonlinearity. On the other hand, the control mechanism can fail when the nonlinearity becomes large, even if only intermittently.

B. Numerical Demonstration

This section demonstrates numerically that Algorithm 1 indeed works well when there are weak nonlinearity, noise, and damping too. Choose the same target functions as (6). The initial condition is the same as before. The oscillator parameters are first chosen to be in TABLE II, in which case we obtain Fig. 6, which shows that trajectory tracking is accomplished to a reasonable extent. Note that the damping, noise and nonlinearity are not too small.

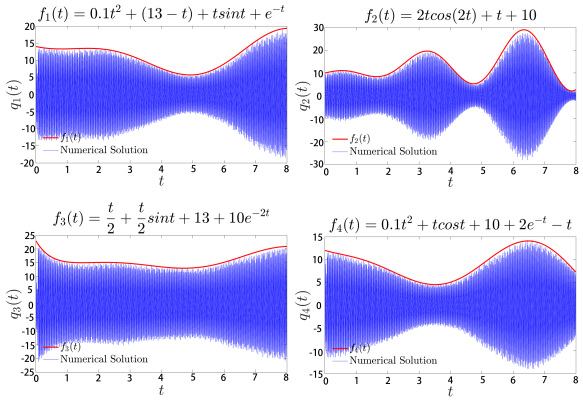

Fig. 6: Tracking of the target amplitude functions (red) when four damped nonlinear noisy oscillators are controlled by Algorithm 1.

We then change the intrinsic frequencies to larger values in TABLE III, and tracking becomes even more accurate as Fig. 7 illustrates. This is precisely what was remarked in Sec. II-B: the error of trajectory-tracking effectively reduces as ω_i increases, because the error is $\mathcal{O}(\varepsilon)$ but ε_i decreases when ω_i increases.

TABLE II: Parameters of oscillators with damping, noise and nonlinearity in Section III-B

ω_1	ω_2	ω_3	ω_4	γ_1	γ_2	γ_3	γ_4
280	290	300	310	4.5	5	5.5	6
μ_1	μ_2	μ_3	μ_4	σ_1	σ_2	σ_3	σ_4
2.5	3	3.5	4	4	3.5	3	2

TABLE III: Parameters of oscillators with damping, noise, nonlinearity, and higher frequencies in Section III-B

ω_1	ω_2	ω_3	ω_4	γ_1	γ_2	γ_3	γ_4
880	*900*	*920*	*940*	4.5	5	5.5	6
μ_1	μ_2	μ_3	μ_4	σ_1	σ_2	σ_3	σ_4
2.5	3	3.5	4	4	3.5	3	2

IV. Conclusion

The dynamical phenomenon of parametric resonance is exploited and shown as a new mechanism for the simultaneous remote control of multiple oscillators. Under reasonable assumptions, a common temporal control signal can enable the amplitude of each high-frequency oscillator to, respectively, follow an arbitrary low frequency trajectory. Based on theoretical analysis, how to design this control signal is specified by Algorithm 1. This control mechanism is robust to perturbations from friction, weak nonlinearity and noise.

V. Appendix

A. A brief recap of averaging and temporal homogenization

Given $\dot{y} = \varepsilon g(y,t)$, $y(t) \in \mathbb{R}^n$, the powerful method of averaging suggests to consider an averaged system $\dot{\bar{y}} = \varepsilon \bar{g}(\bar{y})$, where $\bar{g}(y) := \lim_{T\to\infty} \frac{1}{T}\int_0^T g(y,t)dt$. Under certain conditions (e.g., bounded Lipschitz constant w.r.t. x in g) and assumed existence of $\bar{g}$, averaging theorem quantifies the approximation accuracy as $y(t) = \bar{y}(t) + \mathscr{O}(\delta(\varepsilon))$ till $t = \mathscr{O}(\varepsilon^{-1})$, where $\delta(\varepsilon)$ is an order function that may be as small as ε in some cases but larger in other cases (see e.g., [31] for details and [27] for generalization to SDEs).

Temporal homogenization [10] is more restrictive, but it relaxes required conditions and provided tighter error bound. It works for $\dot{x} = Ax + \varepsilon P(t)x + f(t)$. Such systems can be converted to $\dot{y} = \varepsilon g(y,t)$ via coordinate change. The resulting g may or may not satisfy the Lipschitz condition for the averaging theorem. When it does (e.g., if A is anti-symmetric and $f = 0$), both approaches produce the same approximate system. Otherwise, temporal homogenization can still work. Its full result is in [10], and since this article mainly focuses on cases where $f = 0$, its approximation will be

$$x(t) = e^{At}\left(e^{\varepsilon Bt}x(0) + \mathscr{O}(\varepsilon)\right) \quad \text{till } t = \mathscr{O}(\varepsilon^{-1}) \tag{11}$$

where $B = \lim_{T\to\infty} \frac{1}{T}\int_0^T e^{-At}P(t)e^{At}dt$.

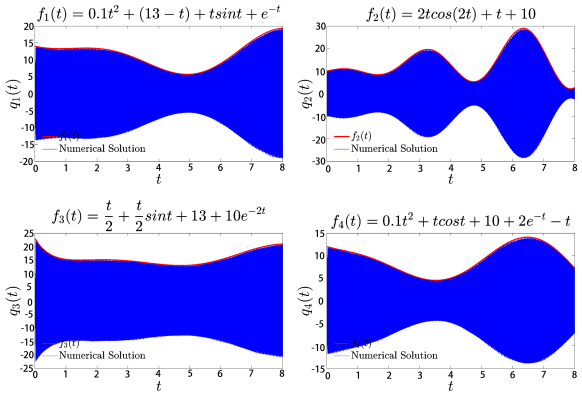

Fig. 7: Further improved tracking of the target amplitude functions (red) when four damped nonlinear noisy oscillators with larger frequencies are controlled by Algorithm 1.

B. Proof of Theorem 1.

Rewrite (4) as

$$\frac{d}{dt}\begin{bmatrix} q_i(t) \\ \dot{q}_i(t)\end{bmatrix} = \Omega\begin{bmatrix} q_i(t) \\ \dot{q}_i(t)\end{bmatrix} + \sum_{j=1}^{n}\varepsilon_j K_j(t)\begin{bmatrix} q_i(t) \\ \dot{q}_i(t)\end{bmatrix} \quad \text{where}$$

$$\Omega = \begin{bmatrix} 0 & 1 \\ -\omega_i^2 & -\gamma_i\end{bmatrix}, \quad K_j(t) = \begin{bmatrix} 0 & 0 \\ -\omega_j^2\cos(2\omega_j t + \theta_j) & 0\end{bmatrix}.$$

Temporal homogenization can approximate the solution (see Section V-A). In its computation, we will only keep $\mathscr{O}(1)$ and $\mathscr{O}(\gamma_i)$ terms due to the assumption that $\gamma_i \ll \omega_i$:

$$e^{\Omega t} = e^{-\frac{\gamma_i t}{2}}\begin{bmatrix} \cos\hat{\omega}_i t + \frac{\gamma_i}{2\hat{\omega}_i}\sin\hat{\omega}_i t & \frac{\sin(\hat{\omega}_i t)}{\hat{\omega}_i} \\ -\frac{\omega_i^2}{\hat{\omega}_i}\sin\hat{\omega}_i t & \cos\hat{\omega}_i t - \frac{\gamma_i}{2\hat{\omega}_i}\sin\hat{\omega}_i t\end{bmatrix}$$

$$+ \mathscr{O}(\gamma_i^2), \quad \text{where} \quad \hat{\omega}_i = \sqrt{\omega_i^2 - \frac{\gamma_i^2}{4}}.$$

$$B = \lim_{T\to\infty}\frac{1}{T}\int_0^T e^{-\Omega t}\sum_{j=1}^{n}K_j(t)e^{\Omega t}dt = \begin{bmatrix} B_{11} & B_{12} \\ B_{21} & B_{22}\end{bmatrix} + \mathscr{O}(\gamma_i^2)$$

$$\text{with} \begin{cases} B_{11} &= -\frac{\sin\theta_i}{2\sqrt{4\omega_i^2-\gamma_i^2}}\omega_i^2 - \frac{\gamma_i}{4\omega_i^2-\gamma_i^2}\cdot\frac{\cos\theta_i}{2}\omega_i^2 \\ B_{12} &= -\frac{\omega_i^2}{4\omega_i^2-\gamma_i^2}\cos\theta_i \\ B_{21} &= -\frac{\omega_i^2}{4}\cos\theta_i + \frac{\gamma_i^2\omega_i^2}{4(4\omega_i^2-\gamma_i^2)}\cos\theta_i + \frac{\gamma_i\omega_i^2}{2\sqrt{4\omega_i^2-\gamma_i^2}}\sin\theta_i \\ B_{22} &= \frac{\sin\theta_i}{2\sqrt{4\omega_i^2-\gamma_i^2}}\omega_i^2 + \frac{\gamma_i}{4\omega_i^2-\gamma_i^2}\cdot\frac{\cos\theta_i}{2}\omega_i^2\end{cases}$$

More algebra leads to

$$\exp(\varepsilon_i Bt) = \begin{bmatrix} A_{11}(t) & A_{12}(t) \\ A_{21}(t) & A_{22}(t)\end{bmatrix} + \mathscr{O}(\gamma_i^2)$$

$$\text{with} \begin{cases} A_{11}(t) &= \frac{2\hat{\omega}_i\cosh\frac{\varepsilon_i t\omega_i^2}{4\hat{\omega}_i} - (\gamma_i\cos\theta_i + 2\hat{\omega}_i\sin\theta_i)\sinh\frac{\varepsilon_i t\omega_i^2}{4\hat{\omega}_i}}{2\hat{\omega}_i} \\ A_{12}(t) &= -\frac{\cos\theta_i\sinh\frac{\varepsilon_i t\omega_i^2}{4\hat{\omega}_i}}{\hat{\omega}_i} \\ A_{21}(t) &= \frac{(\gamma_i^2\cos\theta_i - 4\hat{\omega}_i^2\cos\theta_i + 4\gamma_i\hat{\omega}_i\sin\theta_i)\sinh\frac{\varepsilon_i t\omega_i^2}{4\hat{\omega}_i}}{4\hat{\omega}_i} \\ A_{22}(t) &= \frac{2\hat{\omega}_i\cosh\frac{\varepsilon_i t\omega_i^2}{4\hat{\omega}_i} + (\gamma_i\cos\theta_i + 2\hat{\omega}_i\sin\theta_i)\sinh\frac{\varepsilon_i t\omega_i^2}{4\hat{\omega}_i}}{2\hat{\omega}_i}\end{cases}.$$

The temporal homogenization approximation (11) thus gives

$$q_i(t) = \left(\cosh\left(\frac{\varepsilon_i t\hat{\omega}_i}{4}\right)\left(\sin(\hat{\omega}_i t)(\gamma_i q_i(0) + 2\dot{q}_i(0)) + 2\hat{\omega}_i q_i(0)\cos(\hat{\omega}_i t)\right)\right.$$

$$- \sinh\left(\frac{\varepsilon_i t\hat{\omega}_i}{4}\right)\left((\gamma_i q_i(0) + 2\dot{q}_i(0))\cos(\hat{\omega}_i t + \theta_i)\right.$$

$$\left.\left. + 2\hat{\omega}_i q_i(0)\sin(\hat{\omega}_i t + \theta_i)\right)\right)\frac{e^{-\frac{\gamma_i t}{2}}}{2\hat{\omega}_i} + \mathscr{O}(\varepsilon_i) + \mathscr{O}(\gamma_i^2)$$

Note that cosh and sinh are linear combinations of exponential growth and decay, and carefully choosing θ_i to eliminate one of these two components will prove the theorem.

C. Target functions for producing the GT animation

Let $f_{ij}(t)$ for $1 \le i \le 5$, $1 \le j \le 12$, corresponding to the target functions of the 5×12 blocks, be given by

$$f_{ij}(t) = \begin{cases} h_{ij}(t) & t \in [0,24) \\ l_{ij}(-t+54) & t \in [24,54) \\ l_{ij}(t-54) & t \in [54,84) \end{cases}$$

Note that the shaded blocks in Fig. 8 are not considered as oscillators in our animation. Here:

$$h_{ij}(t) = \begin{cases} 100 & t \in (0, 2(12-j)] \\ g_i(t-24+2j) & t \in (2(12-j), 24] \end{cases}$$

and

$$g_1(t) = \begin{cases} \frac{99}{2}\cos(2\pi t) + \frac{101}{2} & t \in (2,2.5] \cup (7.5,8] \\ & \cup (12,12.5] \cup (17.5,18] \\ 1 & t \in (2.5,7.5] \cup (12.5,17.5] \\ 100 & t \in (0,2] \cup (8,12] \cup (18,24] \end{cases}$$

Besides, $g_i(t), i = 2,3,4,5$ are chosen functions having similar structure as $g_1(t)$. To make *GT* disappear and appear, we let S be the set consisting of the blocks with number $1,2,\cdots,18$ in Fig. 8. The number $k = 1,2,\cdots,18$ denotes the appearing order (handwriting order) here.

- If the block (i,j) is in the set S

$$l_{ij}(t) = \begin{cases} 100 & t \in (0,k] \\ \frac{99}{2} cos(\frac{\pi}{30-k}(t-k)) + \frac{101}{2} & t \in (k,30] \\ 1 & t \in (30,\infty) \end{cases}$$

- For the other blocks, $l_{ij}(t) = 100$, which keep white after *GT* shows up from right.

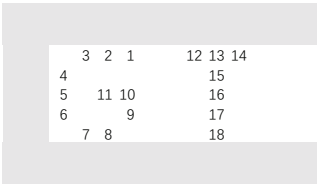

Fig. 8: Set S and the order in the appearance of *GT*

REFERENCES

[1] E. Mathieu, "Mémoire sur le mouvement vibratoire d'une membrane de forme elliptique," *J. Math. Pures Appl.*, vol. 13, pp. 137–203, 1868.

[2] J. Peña-Ramírez, R. H. B. Fey, and H. Nijmeijer, *Parametric Resonance in Dynamical Systems*. Springer New York, 2012.

[3] S. Surappa, S. Satir, and F. Levent Degertekin, "A capacitive ultrasonic transducer based on parametric resonance," *Applied Physics Letters*, vol. 111, no. 4, p. 043503, 2017.

[4] S. Surappa, M. Tao, and F. L. Degertekin, "Analysis and design of capacitive parametric ultrasonic transducers for efficient ultrasonic power transfer based on a 1D lumped model," *IEEE Transactions on Ultrasonics, Ferroelectrics and Frequency Control*, 2018 accepted.

[5] M. Tao, "Simply improved averaging for coupled oscillators and weakly nonlinear waves." Submitted 2018; arXiv:1806.07947.

[6] D. Halperin, T. S. Heydt-Benjamin, K. Fu, T. Kohno, and W. H. Maisel, "Security and privacy for implantable medical devices," *IEEE pervasive computing*, vol. 7, no. 1, 2008.

[7] P. D. Mitcheson, E. M. Yeatman, G. K. Rao, A. S. Holmes, and T. C. Green, "Energy harvesting from human and machine motion for wireless electronic devices," *Proceedings of the IEEE*, vol. 96, no. 9, pp. 1457–1486, 2008.

[8] A. Goldman, *Handbook of modern ferromagnetic materials*, vol. 505. Springer Science & Business Media, 2012.

[9] A. Erturk and D. J. Inman, *Piezoelectric energy harvesting*. John Wiley & Sons, 2011.

[10] M. Tao and H. Owhadi, "Temporal homogenization of linear odes, with applications to parametric super-resonance and energy harvest," *Archive for Rational Mechanics and Analysis*, vol. 220, no. 1, pp. 261–296, 2016.

[11] W.-S. Koon, H. Owhadi, M. Tao, and T. Yanao, "Control of a model of DNA division via parametric resonance," *Chaos*, vol. 23, no. 013117, 2013.

[12] A. Isidori, *Nonlinear control systems*. Springer Science & Business Media, 2013.

[13] F. Bloch, "Nuclear induction," *Phys. Rev.*, vol. 70, pp. 460–474, Oct 1946.

[14] J. Li and N. Khaneja, "Ensemble control of bloch equations," *IEEE Transactions on Automatic Control*, vol. 54, pp. 528–536, March 2009.

[15] J. Li and J. Qi, "Ensemble control of time-invariant linear systems with linear parameter variation," *IEEE Transactions on Automatic Control*, vol. 61, pp. 2808–2820, Oct 2016.

[16] S. Wang and J.-S. Li, "Free-endpoint optimal control of inhomogeneous bilinear ensemble systems," *Automatica*, vol. 95, pp. 306 – 315, 2018.

[17] A. Zlotnik, R. Nagao, I. Z. Kiss, and J.-S. Li, "Phase-selective entrainment of nonlinear oscillator ensembles," *Nature Communications*, vol. 7, pp. 10788 EP –, 03 2016.

[18] A. Jadbabaie, N. Motee, and M. Barahona, "On the stability of the kuramoto model of coupled nonlinear oscillators," in *Proceedings of the 2004 American Control Conference*, vol. 5, pp. 4296–4301 vol.5, June 2004.

[19] A. Papachristodoulou and A. Jadbabaie, "Synchronization in oscillator networks: Switching topologies and non-homogeneous delays," in *Proceedings of the 44th IEEE Conference on Decision and Control*, pp. 5692–5697, Dec 2005.

[20] A. Papachristodoulou and A. Jadbabaie, "Synchonization in oscillator networks with heterogeneous delays, switching topologies and nonlinear dynamics," in *Proceedings of the 45th IEEE Conference on Decision and Control*, pp. 4307–4312, Dec 2006.

[21] A. Papachristodoulou, A. Jadbabaie, and U. Munz, "Effects of delay in multi-agent consensus and oscillator synchronization," *IEEE Transactions on Automatic Control*, vol. 55, pp. 1471–1477, June 2010.

[22] F. Dörfler and F. Bullo, "On the critical coupling for kuramoto oscillators," *SIAM Journal on Applied Dynamical Systems*, vol. 10, no. 3, pp. 1070–1099, 2011.

[23] F. Dörfler and F. Bullo, "Synchronization and transient stability in power networks and nonuniform kuramoto oscillators," *SIAM Journal on Control and Optimization*, vol. 50, no. 3, pp. 1616–1642, 2012.

[24] F. Dörfler, M. Chertkov, and F. Bullo, "Synchronization in complex oscillator networks and smart grids," *Proceedings of the National Academy of Sciences*, vol. 110, p. 2005, 02 2013.

[25] A. E. Motter, S. A. Myers, M. Anghel, and T. Nishikawa, "Spontaneous synchrony in power-grid networks," *Nature Physics*, vol. 9, pp. 191 EP –, 02 2013.

[26] F. Dörfler and F. Bullo, "Synchronization in complex networks of phase oscillators: A survey," *Automatica*, vol. 50, no. 6, pp. 1539 – 1564, 2014.

[27] G. Pavliotis and A. Stuart, *Multiscale methods: averaging and homogenization*. Springer Science & Business Media, 2008.

[28] B. Øksendal, *Stochastic Differential Equations*, pp. 65–84. Berlin, Heidelberg: Springer Berlin Heidelberg, 2003.

[29] M. Freidlin and A. Wentzell, *Random Perturbations of Dynamical Systems*. Springer, third ed., 2012.

[30] C. W. Gardiner, *Handbook of stochastic methods*. Springer Berlin, 3rd ed., 1985.

[31] J. A. Sanders, F. Verhulst, and J. Murdock, *Averaging Methods in Nonlinear Dynamical Systems*. Springer, 2010.